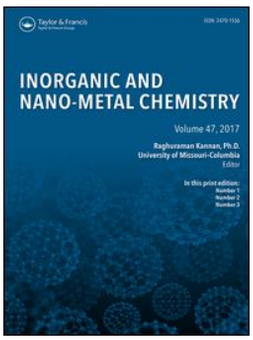


Inorganic and Nano-Metal Chemistry

ISSN: 2470-1556 (Print) 2470-1564 (Online) Journal homepage: http://www.tandfonline.com/loi/lsrt21

# Synthesis, Characterization and Catalytic Performance in Cyclohexane Transformation by $Bi_2O_3$/MCM-41 Nanocomposite Materials

Majid Mozaffari & Amin Ebadi

**To cite this article:** Majid Mozaffari & Amin Ebadi (2017): Synthesis, Characterization and Catalytic Performance in Cyclohexane Transformation by $Bi_2O_3$/MCM-41 Nanocomposite Materials, Inorganic and Nano-Metal Chemistry, DOI: 10.1080/24701556.2017.1357592

**To link to this article:** http://dx.doi.org/10.1080/24701556.2017.1357592

Accepted author version posted online: 31 Jul 2017.

# Synthesis, Characterization and Catalytic Performance in Cyclohexane Transformation by $Bi_2O_3$/MCM-41 Nanocomposite Materials

Majid Mozaffari [1], Amin Ebadi[2,*]

[1]Department of Chemistry, Shahrood Branch, Islamic Azad University, Shahrood, Iran

[2]Department of Chemistry, Kazerun Branch, Islamic Azad University, Kazerun, Iran

[*]Corresponding author:Tel: +98 721 2230505; Fax: +98 721 2230508, *E-mail address:* ebadiamin88@yahoo.com (A. Ebadi).



## ABSTRACT

The nanoparticles of $Bi_2O_3$ supported on mesoporous MCM-41 were prepared in a simple way and were well characterized. The oxidation of cyclohexane to cyclohexanol and cyclohexanone under 1 atmospheric pressure of air in the absence of any solvent and reducing agents with $Bi_2O_3$/MCM-41 nanocomposites were considered. These nanoparticles of $Bi_2O_3$ supported on mesoporous MCM-41 were found to be the very effective catalysts for cyclohexane oxidation with air in a temperature range of 280-370 ˚C. The influences of reaction temperature, the loading amount of $Bi_2O_3$ and space velocity on the oxidation of cyclohexane were also studied, and optimized conditions were investigated.

**Keywords**

Oxidation, Cyclohexane, $Bi_2O_3$/MCM-41, Cyclohexanol, Cyclohexanone

## Introduction

The aerobic oxidation of hydrocarbons is a major goal of today's research in catalysis as selectively oxidized hydrocarbons can be utilized as feedstock for the synthesis of appropriate chemicals.[1-4] Among the oxidation of different alkanes, partial oxidation of cyclohexane to cyclohexanol and cyclohexanone, the intermediates in the making of nylon-6 and nylon-6,6 polymers, have attracted commercial interest.[5] The present commercial process for cyclohexane oxidation is carried out around 150-160°C and high pressure (1-2 MPa) under homogeneous reaction condition that results in the conversion of less than 4% and selectivity of cyclohexanol and cyclohexanone of around 70-85% using metal cobalt salt or metal-boric acid. Because of the relatively harsh condition, low conversion, poor selectivity towards main products and environmental hazards, scientists have been trying to improve aerobic conversion of cyclohexane to favorite products since the 1960s.[6--18]

Supported oxides catalysts are frequently utilized as catalysts in partial oxidation reactions.[19--21] In these catalysts, $Al_2O_3$, $TiO_2$, $SiO_2$, MCM-41 and $ZrO_2$ are generally used as the supports. It is well known that MCM-41 molecular sieve with ordered pore structures and large surface area has been widely used as a carrier in many catalytic reactions.[22--24] Bismuth oxide has wide applications as a catalyst for oxidation reactions.[25] Bulk oxides in general cannot be utilized in oxidation reactions as they impart poor thermal stability that lead to fast degradation of the catalyst. Furthermore, it is also known that bulk oxides leads to high combustion of hydrocarbons to carbon oxides.[26] Yang Lou et al. [27] have studied the complete oxidation of CO with dioxygen in the presence of $Bi_2O_3$ supported on $Co_3O_4$ as catalyst. In another report Huang

and coworkers have employed $Bi_2O_3$ in gadolinia-doped ceria (GDC) as catalyst for direct oxidation of methane. [28]

We reported previously synthesis and catalytic application of γ-alumina supported metallophthalocyanines [MPcs] for cyclohexane oxidation to cyclohexanol and cyclohexanone with air in the absence of solvents and reducing agents. [29] In the present work, we investigated the influence of $Bi_2O_3$/MCM-41 nanocomposites on cyclohexane oxidation reaction in the gas phase under atmospheric pressure and more optimized conditions were obtained in comparison to the catalysts of the previous work. In addition to considering the catalytic properties, in this work, the nanoparticles of $Bi_2O_3$ supported on mesoporous MCM-41 were also synthesized and characterized properly with XRD and SEM. In the previous work, reaction temperature range was of 300-410°C which was a relatively high temperature and MPc/γ-alumina catalysts degraded in the presence of dioxygen with increasing temperature from 340 to 410°C but in the present work, the reaction temperature decreased to 280-370°C that is a relatively mild temperature for industrial applications and thermal stability of the catalysts was retained even up to 370°C and no degradation observed in $Bi_2O_3$/MCM-41 catalyst. This is an advantage of the application of $Bi_2O_3$/MCM-41 nanocomposites.



## Experimental

### *Instrument and Reagents*

The FT-IR spectra were recorded using a Perkin Elmer FT-IR spectrometer by employing KBr pellet technique. X-ray powder diffraction (XRD) patterns of the samples were recorded using a Bruker Advance D8 Diffractometer with Cu $K_\alpha$ radiation ($\lambda$ = 0.154 nm). BET surface area was

obtained from $N_2$ adsorption isotherms at 77 K by a Strohlien. Scanning electron microscopy (SEM) observations were performed by means of a Holland Philips XL30 microscope. TEM images obtained on a Philips CM 200 FEG/HRTEM (high-resolution transmission electron microscope) instrument operating at 200 Kv. The nanocomposites analysis was done by Energy dispersive X-ray (EDAX) on a TESCAN MIRA3 FE-SEM. GC analysis of cyclohexane oxidation products was performed on a Shimadzu 8A, using authentic samples equipped with a TCD detector using OV-17, Propak-N, packed (2 m) columns and Helium as the carrier gas. The products of oxidation were measured by GC--MS model of Thermoquest-Finnigan Trace, equipped with a DB-1 fused silica column (with a length of 60 m and internal diameter of 0.25 mm and film thickness of 0.25 μm) with He as the carrier gas. All reagents used were of commercial grade and were obtained from Merck. No impurities were found in the cyclohexane before the oxidation reaction.

***Preparation of $Bi_2O_3$ / MCM-41 Nanocomposites***

Sodium silicate solution (25.5 - 28.5 wt % $SiO_2$ and 7.5 - 8.5 wt % $Na_2O$, MERK), cetyltrimethylammonium bromide (CTAB, 99%, BDH), acetic acid glacial (100%, analytical regent grade), $Bi(NO_3)_3{\cdot}5H_2O$ (Aldrich), $HNO_3$ (Fischer) and ammonium hydroxide solution utilized as starting chemicals, all were of analytical grade.

Mesoporous MCM-41 silica was prepared using a gel mixture with a combination of $4SiO_2$: 1CTAB: $250H_2O$, which was described in the literature.[30] A required amount of the CTAB was dissolved slowly in a suitable amount of deionized water and sodium silicate solution and was stirred with an electro-magnetic stirrer for 30 min. By adding acetic acid drop wise, pH of the

resultant mixture reached to 10 and the formed gel was transferred to a polypropylene bottle and refluxed at 100°C for 24 h. After cooling and adjusting the pH at 10 with acetic acid, the mixture was refluxed again for 24 h at 100°C. The pH adjustment and subsequent heating operations were repeated several times for 5 days. After the gel was formed, it was filtered and washed by deionized water and dried in an oven to form white MCM-41 nanopowders.

Anchoring of $Bi_2O_3$ nanoparticles on MCM-41 was carried out by a simple impregnation method. 1.0 g mesoporous MCM-41 was mixed with n g (n = 0.11, 0.21, 0.31) $Bi(NO_3)_3.5H_2O$ dissolved in 30 mL 0.53 mol/l nitric acid. Ammonium hydroxide solution was dropped into the mixing solution under constant stirring till pH reached to 6-7. After stirring for 2 h, at room temperature, the resulting precipitate was washed repeatedly with deionized water and dried in an oven at 100°C overnight and calcined in flowing air at 450°C for 2 h.

***Experimental Procedure***

A vertical fixed-bed glass reactor with 9 cm length and internal diameter of 1.5 cm operating under 1 atm pressure was utilized for the partial oxidation of cyclohexane with air. About 1 g of the supported bismuth oxide sample with 50-70 mesh was placed on a sinter glass and fed with a 50 mL cyclohexane syringe by the automatic injector (Fresenius injectomats) at the desired temperature. The reactor was placed inside a temperature controlled heating jacket and a thermocouple, placed at the center of the catalyst bed was utilized to control the furnace temperature. The liquid products were collected by passing the hot gasses through a water-cool condenser. The range of reaction temperature was 280-370°C, air was injected at 30 mL/min velocity and cyclohexane at 2 mL/h velocity at atmospheric pressure. The time of reaction of 3 h

was selected and a dual channel (Shimadzu Model 8A) gas chromatograph (GC) was utilized online for analyzing the products of oxidation.

**Results and Discussion**

***Structural Characterization***

Figure 1 shows low angle X-ray diffraction patterns of obtained MCM-41 and synthesized nanocomposite samples $Bi_2O_3$/MCM-41. While the wide angle X-ray patterns for the prepared MCM-41+10% $Bi_2O_3$ nanocomposite is shown in Figure 2. The very intense peak appeared at low angle ($2\theta = 2.55$) on the Figure 1 is assigned to reflections at (100) and two other additional picks with low intensities at (110) and (200) reflections indicate to the regular pore structure of MCM-41 and can be attributed to quasi-two-dimensional hexagonal lattice of MCM-41.[31] On dispersing $Bi_2O_3$ over MCM-41, a reduction in the peak intensity of the characteristic (100) plan is overcoming while, at higher bismuth oxide loadings samples, the peaks of (110) and (200) planes tend to merge with the base line.

Decrease in the intensity can be attributed to the pores covering effects that reduce the scattering contrast between the pores and the framework of MCM-41 sample. The wide angle X-ray diffraction patterns, Figure 2, show the characteristic peaks appeared at $2\theta = 26.94$, $2\theta = 27.40$ and $2\theta = 33.25$ and confirm the presence of $Bi_2O_3$ phase in $Bi_2O_3$ / MCM-41 nanocomposites. In our case, all diffraction peaks are assigned to $Bi_2O_3$ crystallized in monoclinic form corresponding to JCPDS files no. 41-1449. The intensity of this peaks increases with increasing $Bi_2O_3$ loading indicating the agglomeration of the particles at higher loadings. This indicates that $Bi_2O_3$ nanoparticles remains mainly on the external surface since the bismuth oxide has a high

kinetic diameter, which facilitates the coverage of the hexagonal channels of MCM-41 pores. This interpretation is in agreement with XRD results in the low angle region that showed the decrease in all peaks associated with MCM-41 structure. According to the Debye- Scherrer's equation: $D = k\lambda / \beta \cos \theta$

Where D is the average crystallite size, k is a constant equal to o.9, λ is the X-ray wavelength equal to 0.15406 nm and β is the half-peak width, the mean crystallite size of the as-synthesized products calculated according to this equation is about 15 nm.

Figure 3 shows the FT-IR spectra of MCM-41, $Bi_2O_3$ and MCM-41+10% $Bi_2O_3$ samples. In the spectrum of the raw MCM-41 (Figure 3(a)), a broad band at 1075 $cm^{-1}$ is due to asymmetric stretching vibrations of Si-O-Si bridges and the absorption bands observed at 467 and 812 $cm^{-1}$ is assigned to the asymmetric and symmetric Si-O stretching vibrations.[32,33] In the spectrum of $Bi_2O_3$ (Figure 3(b)), the FT-IR spectra of crystalline α-$Bi_2O_3$ present absorption bands at: 510 and 540 $cm^{-1}$, specific to the vibrations of Bi-O bonds in $BiO_6$ octahedral units and the absorption bands at: 715 and 880 $cm^{-1}$, characteristic of the vibrations of Bi-O bonds in $BiO_3$ pyramidal units.[34, 35] In the spectrum of MCM-41+10% $Bi_2O_3$ sample (Figure 3(c)), a broad band at 1075 $cm^{-1}$ and a band at 812 $cm^{-1}$ were corresponding to the asymmetric and symmetric Si-O stretching vibrations. The band at 715 $cm^{-1}$ due to symmetric stretching vibrations of Bi-O bonds in $BiO_3$ pyramidal units confirm the presence of $Bi_2O_3$ phase in $Bi_2O_3$ / MCM-41 nanocomposites.

The scanning electronic microscopy (SEM) results of the supported catalysts are presented in Figure 4. The formation of spherical particles with the diameter varying between 50 to 90 nm

was observed for MCM-41, which exhibited also a smooth surface and a homogeneous particle size distribution. However, from (Figure 4b, c and d) the surface of the $Bi_2O_3$/MCM-41 nanocomposites showed rough. In addition, the impregnation of $Bi_2O_3$ nanoparticles on MCM-41 generated an increase in the number and size of these nanocomposites but also the formation of small like spherical aggregates with widths of approximately 0.5 µm.

Transmission electron microscopy (TEM) images of MCM-41 and 10% $Bi_2O_3$/MCM-41 nanocomposite are illustrated in Figure 5. The mesoporous framework of MCM-41 exposed well-ordered hexagonal array of cylindrical channels and well-defined channels and walls (Figure 5(a)). This is entirely consistent with the XRD results. The distribution of black spots with a size between 15-20 nm can be attributed to the $Bi_2O_3$ nanoparticles, which is in agreement with its measurements obtained by XRD (Figure 5(b)).

Figure 6 shows the energy-dispersive X-ray (EDX) spectra of $Bi_2O_3$/MCM-41 nanocomposites. The result was analyzed on a small surface on the as-prepared catalysts. Peaks of atomic O, Si and Bi were observed. It reveals that the $Bi_2O_3$ nanoparticles has been successfully grown on the MCM-41 mesoporous. The EDX spectra revealed that the nanocomposites contained 4.68%, 10.87% and 15.37% Bi which is very close to the stoichiometric percent. Also, no other impurity peak is found in EDX spectra, indicating that the products are pure.

Specific surface area measured with BET method was 1081 $m^2/g$ for MCM-41, 1019 $m^2/g$ for 5 wt.% $Bi_2O_3$/MCM-41, 881 $m^2/g$ for 10 wt.% $Bi_2O_3$/MCM-41 and 792 $m^2/g$ for 15 wt.% $Bi_2O_3$/MCM-41.

***Air Oxidation of Cyclohexane***

The cyclohexane oxidation reaction catalyzed by the nanoparticles of $Bi_2O_3$ supported on mesoporous MCM-41 with air was as follows:

This reaction was operated at a temperature range of 280-370°C with molecular oxygen under 1 atmospheric pressure in the absence of solvents and co-catalysts. In the presence of 10 wt.% $Bi_2O_3$/MCM-41, conversion percentage of cyclohexane was 27.56% with selectivity of 43.45% for cyclohexanol + cyclohexanone at 310°C, a relatively mild system for industry. The products of cyclohexane oxidation catalyzed by supported $Bi_2O_3$ were mostly cyclohexanol and cyclohexanone. GC-MS analysis data showed that there were small amounts of cyclohexene, cyclohexadiene, 5-hexen-1-al, CO and $CO_2$. cyclohexene was formed by dehydrogenation of cyclohexane. In this regard 22.10% of cyclohexene was obtained. The product distribution for 10 wt.% $Bi_2O_3$/MCM-41 is listed in Table 1. Zhou et al. [36] have reported that with gold nanoparticles on MCM-41 catalyst and in autoclave a cyclohexane conversion percent of around 12.0% with 60.0% selectivity toward cyclohexanone was obtained using molecular oxygen as oxidant. In another report Sun and coworker [37] have used MCM-41 encapsulated Co(III)-porphyrin complex, in the reaction of cyclohexane oxidation. The results show that the reactivity about 10.38% conversion of cyclohexane and 98.08% cyclohexanol selectivity with oxygen as the oxidizing agent.

Contrastive experiment results revealed that cyclohexane aerobic oxidation with air did not happen in the absence of the catalyst under similar reaction condition, and MCM-41 encapsulated $Bi_2O_3$ has shown better catalytic power for cyclohexane oxidation with air than the corresponding unsupported $Bi_2O_3$.

When the reaction was catalyzed with MCM-41 without any $Bi_2O_3$, cyclohexane conversion and selectivity of the products reduced considerably in comparison with $Bi_2O_3$ supported on MCM-41. This revealed that the active species which were responsible for the oxidation of cyclohexane were loaded $Bi_2O_3$ on the support, because no reactivity and activity towards cyclohexane oxidation were reported when we use only MCM-41 as a catalyst.

The stability of the catalyst was tested at the end of the reaction, and the result confirms that stability of the catalyst is good, decomposition of nanocomposite was negligible and its reactivity was preserved. The stability of the catalysts were investigated by XRD and FT-IR spectra. Trace a in Figure 7 demonstrates FT-IR spectrum of the freshly prepared 10% of $Bi_2O_3$/MCM-41 before the reaction test. Trace b in Figure 7 is for the 10% of $Bi_2O_3$/MCM-41 after the reaction test was performed at 370°C. FT-IR spectra shows that the absorption bands of 10% $Bi_2O_3$/MCM-41 nanocomposite before and after catalytic procedure are completely similar and revealed that the catalyst remained unchanged. Similar low-angle X-ray diffraction patterns were obtained for the catalyst before and after the reaction test (Figure 8) and alone the intensities of peaks in the used catalyst are reduced, indicating the stability of nanocomposites.

***The Influences of Temperature on Cyclohexane Oxidation Reaction***

In order to investigate the effect of temperature on the oxidation, we carried out the reaction under different temperatures, such as 280, 310, 340 and 370°C. It showed that the reaction temperature gives great influence on the oxidation. The results are concluded in Table 2. With regard to the subject that importance of selectivity is more than the conversion percent, all three catalysts showed their best performance in 310°C. Figures 9 and 10 shows how cyclohexane

conversion and the selectivities of the products changed with reaction temperature in the presence of various catalysts, respectively.

As shown in Table 2 the rise in reaction temperature from 280 to 370°C, increased the conversion of cyclohexane and the highest value of the conversion was obtained when reaction temperature was increased to 370°C. As for the distribution of the products, with increasing reaction temperature from 280 to 310°C, the selectivity of cyclohexanone and cyclohexanol increased and reached its maximum in 310°C. When reaction temperature was increased from 310°C to 370°C, selectivity of the cyclohexanone and cyclohexanol decreased considerably. Moreover, in higher temperatures more CO and $CO_2$ were formed that were the products of full oxidation. The lessening of selectivity at higher temperatures may be as a result of oxidative destruction of the products.

***The Influences of the Loading Amount of Bismuth Oxide on Cyclohexane Oxidation Reaction***

For investigating of the loading effect $Bi_2O_3$ on the conversion and selectivity of the products, three catalysts were tested. In Table 2, details of the conversion and selectivity of the products for each catalyst are shown. It is observed that maximum conversion and selectivity for desired products occur with the catalyst of 10 wt.% $Bi_2O_3$. It is known that $Bi_2O_3$ nanoparticles can be highly dispersed on mesoporous MCM-41 at 10 wt.% loading. The reduction of conversion of cyclohexane and selectivity for the main products of the catalyst with higher loadings than 10 wt.% maybe due to a distortion of the long range ordering of the mesoporous structure and/or badly built hexagonal array and more decrease of the specific surface area of the catalyst. Under

these reaction conditions, the order of catalytic activities is as follows: 10 wt.% $Bi_2O_3$ / MCM-41 > 15 wt.% $Bi_2O_3$ / MCM-41 > 5 wt.% $Bi_2O_3$ / MCM-41.

***The Influences of Space Velocity on Cyclohexane Oxidation Reaction***

The effects of space velocity on the conversion of cyclohexane and selectivity of cyclohexanol and cyclohexanone can be seen in table 3. Space velocity refers to the quotient of the entering volumetric flow rate of substrate divided by the catalyst volume which indicates how many reactor volumes of feed can be reacted in a unit time. Space velocity is an indicator for contact time of substrate with the catalyst. In space velocities more than 3299 $h^{-1}$ (rate of cyclohexane injection = 2.5 mL/h and rate of air flow = 30 mL/min), contact time of cyclohexane with catalyst is short and conversion percent and selectivity of cyclohexanol and cyclohexanone are low. Thus, in space velocities lower than 3004 $h^{-1}$ (rate of cyclohexane injection = 1.5 mL/h and rate of air flow = 30 mL/min), contact time appears too much, chief oxidation products are CO and $CO_2$ and selectivity of cyclohexanol and cyclohexanone is reduced. When $O_2$ flow rate is lowered, the conversion of cyclohexane and selectivity for the main products also reduced i.e. for space velocity 2297 $h^{-1}$ (rate of cyclohexane injection = 2 mL/h and rate of air flow = 20 mL/min). The best combination for high conversion percent and good selectivity for cyclohexanol and cyclohexanone was attained at 3151 $h^{-1}$ space velocity (rate of cyclohexane injection = 2 mL/h and rate of air flow = 30 mL/min). Thus, contact time of the reactants with catalyst appears a main factor for high conversion and specificity of the products.

**Discussion**

In order to explain how the oxidation occurred, based on the literatures [38], it seems that oxidation of cyclohexane using $O_2$ as oxidant proceeds via a radical-chain sequence mechanism as shown in Scheme 1.

**Conclusions**

This work investigates the preparation, characterization and activity of $Bi_2O_3$/MCM-41 nanocomposites for oxidation of cyclohexane with air, in the absence of any reductant, solvent and co-catalyst. The nanoparticles of $Bi_2O_3$ supported on mesoporous MCM-41 were found to be potentially active and selective catalysts for the partial oxidation of cyclohexane to desired products. Bismuth oxide supported on mesoporous MCM-41 resists destructive oxidation and can be easily separated after the reaction. Maybe, it is more suitable for industrial applications than the equivalent unsupported catalyst. The factors that influence the oxidation were also well investigated. It can be concluded that the optimum reaction condition of the oxidation is: catalyst 10 wt.% $Bi_2O_3$ / MCM-41, 1 atm air, space velocity 3151 $h^{-1}$ and temperature 310°C.

**Acknowledgements**

The authors are grateful to the Research Council of Shahrood and Kazerun branch, Islamic Azad University for financial assistance.

References

1. Yang, G.; Zhang, Q.; Miao, H.; Tong, X.; Xu, J. Selective organocatalytic oxygenation of hydrocarbons by dioxygen using anthraquinones and *N*-hydroxyphthalimide. *Org. Lett*. **2005**, 7, 263-266.

2. Punniyamurthy, T.; Velusamy, S.; Iqbal, J. Recent advances in transition metal catalyzed oxidation of organic substrates with molecular oxygen. *Chem. Rev*. **2005**, 105, 2329-2364.

3. Jones, W. D. Hydrocarbon chemistry:enhanced: conquering the carbon-hydrogen bond. *Science* **2000**, 287, 1942-1943.

4. Zhang, P.; Lu, H.; Zhou, Y.; Zhang, L.; Wu, Z.; Yang, S.; Shi, H.; Zhu, Q.; Chen, Y.; Dai, S. Mesoporous $MnCeO_x$ solid solutions for low temperature and selective oxidation of hydrocarbons. *Nature Commun*. **2015**, 6, 8446-8456.

5. Du, Y.; Xiong, Y.; Li, J.; Yang, X. Selective oxidation of cyclohexane with hydrogen peroxide in the presence of copper pyrophosphate. *J. Mol. Catal. A: Chem*. **2009**, 298, 12-16.



 

*6. Carabineiro, S. A. C.; Martins, L. M. D. R. S.; Avalos-Borja, M.; Buijnsters, J. G.; Pombeiro, A. J. L.; Figueiredo, J. L. Gold nanoparticles supported on carbon materials for cyclohexane oxidation with hydrogen peroxide.* Appl. Catal. A: Gen. ***2013**, 467, 279-290.*

***7. Pokutsa, A.; Kubaj, Y.; Zaborovskyi, A.; Maksym, D.; Muzart, J.; Sobkowiak, A. The effect of oxalic acid and glyoxal on the $VO(acac)_2$-catalyzed cyclohexane oxidation with $H_2O_2$.*** **Appl. Catal. A: Gen.** *2010**, 390, 190-194.***

8. Liu, X.; He, J.; Yang, L.; Wang, Y.; Zhang, S.; Wang, W.; Wang, J. Liquid-phase oxidation of cyclohexane to cyclohexanone over cobalt-doped SBA-3. *Catal. Commun.* **2010**, 11, 710-714.

9. Jatupisarnpong, J.; Trakarnpruk, W. Transition metal-substituted polyoxometalates supported on MCM-41 as catalysts in the oxidation of cyclohexane and cyclooctane with $H_2O_2$. *Mendeleev Commun*. **2012**, 22, 152-153.

10. Wu, P.; Bai, P.; Loh, K. P.; Zhao, X. S. Au nanoparticles dispersed on functionalized mesoporous silica for selective oxidation of cyclohexane. C*atal. Today* **2010**, 158, 220-227.

***11. Mistri, R.; Maiti, S.; Llorca, J.; Dominguez, M.; Mandal, T. K.; Mohanty, P.; Ray, B. C.; Gayen, A. Copper ion substituted hercynite ($Cu_{0.03}Fe_{0.97}Al_2O_4$): A highly active catalyst for liquid phase oxidation of cyclohexane.*** **Appl. Catal. A: Gen.** *2014**, 485, 40-50.***

12. Martins, L. M. D. R. S.; Martins, A.; Alegria, E. C. B. A.; Carvalho, A. P.; Pombeiro, A. J. L. Efficient cyclohexane oxidation with hydrogen peroxide catalysed by a c-scorpionate iron(II) complex immobilized on desilicated mor zeolite. *Appl. Catal. A: Gen.* **2013**, 464-465, 43-50.

13. **Huang, G.; Luo, Z-C.; Xiang, F.; Cao, X.; Guo, Y-A.; Jiang, Y-X. Catalysis behavior of boehmite-supported iron tetraphenylporphyrins with nitro and methoxyl substituents for the aerobic oxidation of cyclohexane. J. Mol. Catal. A: Chem.** 2011**, 340, 60-64.**

14. **Fu, Y.; Zhan, W.; Guo, Y.; Wang, Y.; Liu, X.; Guo, Y.; Wang, Y.; Lu, G. Effect of surface functionalization of cerium-doped MCM-48 on its catalytic performance for liquid-phase free-solvent oxidation of cyclohexane with molecular oxygen. Micropor. Mesopor. Mater.** 2015**, 214, 101-107.**

15. **Wu, M.; Zhan, W.; Guo, Y.; Guo, Y.; Wang, Y.; Wang, L.; Lu, G. An effective Mn-Co mixed oxide catalyst for the solvent-free selective oxidation of cyclohexane with molecular oxygen. Appl. Catal. A: Gen.** 2016**, 523, 97-106.**

16. **Machado, P. M. A.; Lube, L. M.; Tiradentes, M. D. E.; Fernandes, C.; Gomes, C. A.; Stumbo, A. M.; San Gil, R. A. S.; Visentin, L. C.; Sanchez, D. R.; Frescura, V. L. A.; Silva, J. S. A.; Horn Jr, A. Synthesis, characterization and activity of homogeneous and heterogeneous ($SiO_2$, NaY, MCM-41) iron(III) catalysts on cyclohexane and cyclohexene oxidation. Appl. Catal. A: Gen.** 2015**, 507, 119-129.**

17. **Yuan, X.; Shan, G.; Li, L.; Wu, J.; Luo, H. Methyl group modified MCM-41 supported schiff-base cobalt complex and its catalytic performance in cyclohexane oxidation. Catal. Lett.** 2015**, 145, 868-874.**

***18. Zhang, W.; Lu, G.; Guo, Y.; Guo, Y.; Wang, Y.; Wang, Y.; Zhang, Z.; Liu, X. Synthesis of cerium-doped MCM-48 molecular sieves and its catalytic performance for selective oxidation of cyclohexane.*** **J. Rare Earths.** *2008**, 26, 515-522.***

19. Wu, P. P.; Bai, P.; Lei, Z. B.; Loh, K. P.; Zhao, X. S. Gold nanoparticles supported on functionalized mesoporous silica for selective oxidation of cyclohexane, *Micropor. Mesopor. Mat*. **2011**, 141, 222-230.

20. Mishra, G. S.; Kumar, A.; Mukhopadhyay, S.; Tavares, P. B. Novel alkoxysilane pentacoordinate OV(IV) complexes as supported catalysts for cyclohexane oxidation with dioxygen. *Appl. Catal. A: Gen*. **2010**, 384, 136-146.

21. Thomas, J. M.; Raja, R.; Sankar, G.; Bell, R. G. Molecular sieve catalysts for the aerobic selective oxidation of hydrocarbons. *Stud. Surf. Sci. Catal*. **2000**, 130, 887- 892.

22. Zhang, D. S.; Wang, R. J.; Yang, X. X. Beckmann rearrangement of cyclohexanone oxime over Al-MCM-41 and P modified Al-MCM-41 molecular sieves. *Catal. Commun.* **2011**, 12, 399-402.

23. Jha, A.; Garade, A. C.; Mirajkar, S. P.; Rode, C. V. MCM-41 supported phosphotungstic acid for the hydroxyalkylation of phenol to phenolphthalein. *Ind. Eng. Chem. Res*. **2012**, 51, 3916-3922.

24. Ambrogi, V.; Latterini, L.; Marmottini, F.; Pagano, C.; Ricci, M. Mesoporous silicate MCM-41 as a particulate carrier for octyl methoxycinnamate: sunscreen release and photostability. *J. Pharmaceutical Sci*. **2013**, 102, 1468-1475.

**25. Malik, P.; Chakraborty, D. $Bi_2O_3$-catalyzed oxidation of aldehydes with *t*-BuOOH.**

*Tetrahedron Lett*. **2010**, 51, 3521-3523.

26. Routray, K.; Reddy, K. R. S. K.; Deo, G. Oxidative dehydrogenation of propane on $V_2O_5/Al_2O_3$ and $V_2O_5/TiO_2$ catalysts: understanding the effect of support by parameter estimation. *Appl. Catal. A: Gen*. **2004**, 265, 103-113.

27. Lou, Y.; Wang, L.; Zhang, Y.; Zhao, Z.; Zhang, Z.; Lu, G.; Guo, Y. The effects of $Bi_2O_3$ on the CO oxidation over $Co_3O_4$. *Catal. Today* **2011**, 175, 610- 614.

28. Huang, T-J.; Li, J-F. Direct methane oxidation over a $Bi_2O_3$ --GDC system. *J. Power Sources* **2007**, 173, 959-964.

29. Ebadi, A.; Safari N.; Peyrovi, M. H. Aerobic oxidation of cyclohexane with γ-alumina supported metallophthalocyanines in the gas phase. *Appl. Catal. A: Gen*. **2007**, 321, 135-139.

30. Sadjadi, M. S.; Mozaffari, M.; Enhessari, M.; Zare, K. Effects of $NiTiO_3$ nanoparticles supported by mesoporous MCM-41 on photoreduction of methylene blue under UV and visible light irradiation. *Superlattices Microstruct*. **2010**, 47, 685-694.

31. Kresge, C. T.; Leonowicz, M. E.; Roth, W. J.; Vartuli, J. C.; Beck, J. S. Ordered mesoporous molecular sieves synthesized by a liquid-crystal template mechanism. *Nature* **1992**, 359, 710-712.

32. Romero, A. A.; Alba, M. D.; Zhou, W.; Klinowski, J. Synthesis and characterization of the mesoporous silicate molecular sieve MCM-48. *J. Phys. Chem. B* **1997**, 101, 5294-5300.

33. Takahashi, R.; Sato, S.; Sodesawa, T.; Kawakita, M.; Ogura, K. High surface-area silica with controlled pore size prepared from nanocomposite of silica and citric acid. *J. Phys. Chem. B* **2000**, 104, 12184-12191.

34. Dimitrov, V.; Dimitriev, Y.; Montenero, A. IR spectra and structure of $V_2O_5/GeO_2/Bi_2O_3$ glasses. *J. Non -- Cryst. Solids* **1994**, 180, 51-57.

35. Iordanova, R.; Dimitriev, Y.; Dimitrov, V.; Kassabov, S.; Klissurski, D. Glass formation and structure in the $V_2O_5/Bi_2O_3/Fe_2O_3$ glasses. *J. Non -- Cryst. Solids* **1996**, 204, 141-150.

36. Zhou, J.; Yang, X.; Wang, Y.; Chen, W. An efficient oxidation of cyclohexane over $Au@TiO_2$/MCM-41 catalyst prepared by photocatalytic reduction method using molecular oxygen as oxidant. *Catal. Commun*. **2014**, 46, 228-233.

37. Luo, Sh.; Sun, J. Preparation of bimodal MCM-41 encapsulated Co(III)-porphyrin complex and its catalytic properties in cyclohexane oxidation. *Stud. Surf. Sci. Catal*. **2007**, 165, 459-462.

38. Oconnor, R. P.; Schmidt, L. D. Catalytic partial oxidation of cyclohexane in a single-gauze reactor. *J. Catal*. **2000**, 191, 245-256.



 

**Table 1.** Product distribution for cyclohexane partial oxidation by air at T = 310°C, P = 1 atm, rate of cyclohexane injection = 2 mL/h, rate of air flow = 30 mL/min and catalyst 10 wt.% $Bi_2O_3$/MCM-41

| Product[a] | Selectivity (%) |
|---|---|
| Cyclohexene | 22.10 |
| Cyclohexanone | 23.14 |
| Cyclohexanol | 20.31 |
| $CO_2$ | 11.25 |
| Cyclohexadiene | 6.77 |
| CO | 7.09 |
| 5-Hexen 1 al | 6.31 |
| Methanol | 1.08 |
| Ethanol | 0.75 |
| Phenol | 0.68 |
| Phermaldehide | 0.52 |

[a] Only products with ≥0.5% selectivity are shown.



 

**Table 2.** The effect of reaction temperature on aerobic oxidation[a] of cyclohexane

| Catalyst | Temperature | Conversion | Selectivity products[b] (%) | | | | | |
|---|---|---|---|---|---|---|---|---|
| | (°C) | (%) | A | B | C | D | E | F |
| 5% $Bi_2O_3$/MCM-41 | 280 | 14.23 | 21.67 | 16.21 | 15.52 | 7.58 | 6.76 | 29.01 |
| 5% $Bi_2O_3$/MCM-41 | 310 | 20.46 | 22.19 | 17.48 | 16.88 | 7.15 | 7.53 | 25.41 |
| 5% $Bi_2O_3$/MCM-41 | 340 | 22.37 | 24.76 | 13.24 | 12.98 | 9.71 | 7.37 | 28.14 |
| 5% $Bi_2O_3$/MCM-41 | 370 | 25.43 | 27.35 | 10.76 | 9.66 | 9.83 | 6.44 | 32.49 |
| 10% $Bi_2O_3$/MCM-41 | 280 | 19.75 | 20.16 | 20.25 | 18.62 | 7.16 | 7.23 | 22.78 |
| 10% $Bi_2O_3$/MCM-41 | 310 | 27.56 | 22.10 | 23.14 | 20.31 | 6.77 | 6.31 | 18.34 |
| 10% $Bi_2O_3$/MCM-41 | 340 | 29.81 | 25.36 | 17.82 | 15.47 | 8.72 | 6.86 | 22.27 |
| 10% $Bi_2O_3$/MCM-41 | 370 | 31.76 | 26.02 | 14.32 | 13.71 | 9.47 | 7.35 | 26.08 |
| 15% $Bi_2O_3$/MCM-41 | 280 | 15.21 | 21.43 | 17.26 | 16.30 | 7.26 | 7.76 | 26.23 |
| 15% $Bi_2O_3$/MCM-41 | 310 | 22.89 | 23.31 | 19.96 | 18.92 | 7.43 | 6.37 | 21.01 |
| 15% $Bi_2O_3$/MCM-41 | 340 | 24.11 | 24.32 | 15.46 | 14.23 | 8.37 | 7.49 | 26.33 |
| 15% $Bi_2O_3$/MCM-41 | 370 | 27.93 | 26.71 | 11.78 | 10.12 | 9.26 | 8.19 | 30.44 |
| $Bi_2O_3$ | 280 | 11.66 | 21.17 | 13.21 | 11.78 | 6.61 | 5.10 | 38.53 |
| $Bi_2O_3$ | 310 | 15.52 | 11.22 | 11.25 | 9.63 | 6.31 | 5.36 | 52.63 |
| $Bi_2O_3$ | 340 | 19.73 | 12.45 | 6.67 | 4.14 | 7.22 | 5.39 | 60.35 |
| $Bi_2O_3$ | 370 | 23.43 | 9.85 | 4.15 | 2.05 | 5.76 | 6.35 | 68.25 |

[a] Catalyst = X% $Bi_2O_3$/MCM-41 nanocomposites, catalyst weight = 1 g, reaction time = 3 h, P = 1 atm, rate of cyclohexane injection = 2 mL/h and rate of air flow = 30 mL/min.

[b] A = cyclohexene, B = cyclohexanone, C = cyclohexanol, D = cyclohexadiene, E = 5-hexen 1-al, F = $CO_x$.



 

**Table 3.** The effect of space velocity on the conversion of cyclohexane and selectivity of cyclohexanol and cyclohexanone formation[a]

| Space velocity ($h^{-1}$) | Conversion (%) | Selectivity (%) |
|---|---|---|
| 2297 | 22.14 | 21.36 |
| 3004 | 33.44 | 34.67 |
| 3151 | 27.56 | 43.45 |
| 3299 | 20.37 | 37.85 |
| 4006 | 14.11 | 32.36 |

[a] Catalyst = 10 wt.% $Bi_2O_3$/MCM-41, T = 310°C, catalyst volume ≈ 1.5 mL, catalyst weight = 1 g, reaction time = 3 h, P = 1 atm

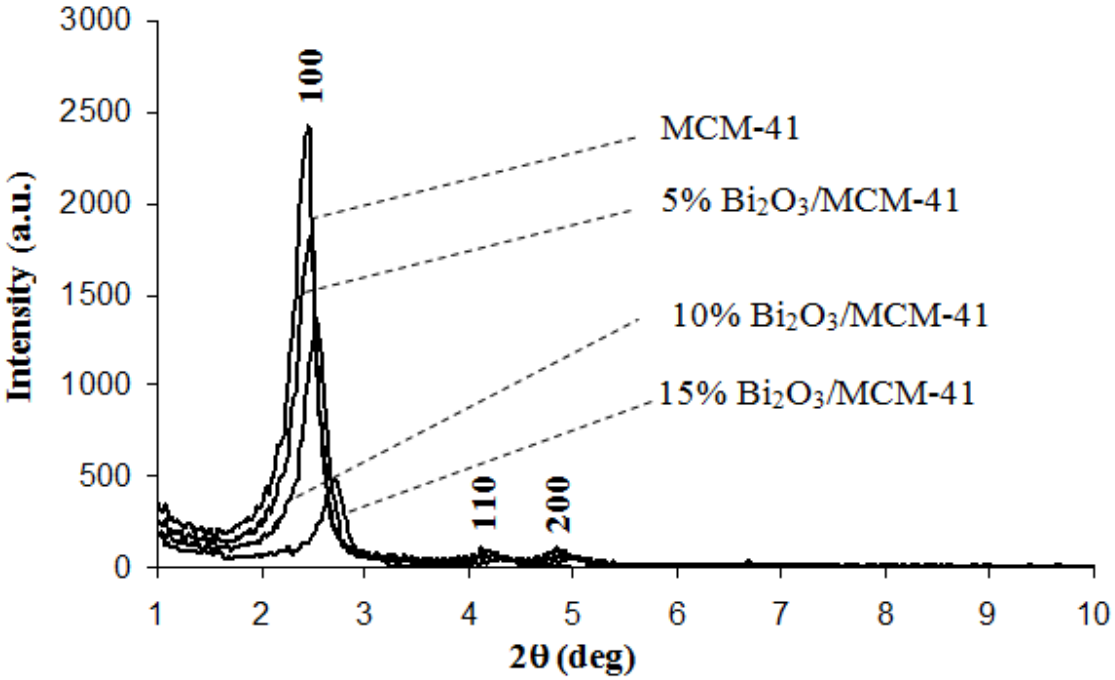


**Fig. 1.** XRD patterns of samples MCM-41 and $Bi_2O_3$/MCM-41 nanocomposites.

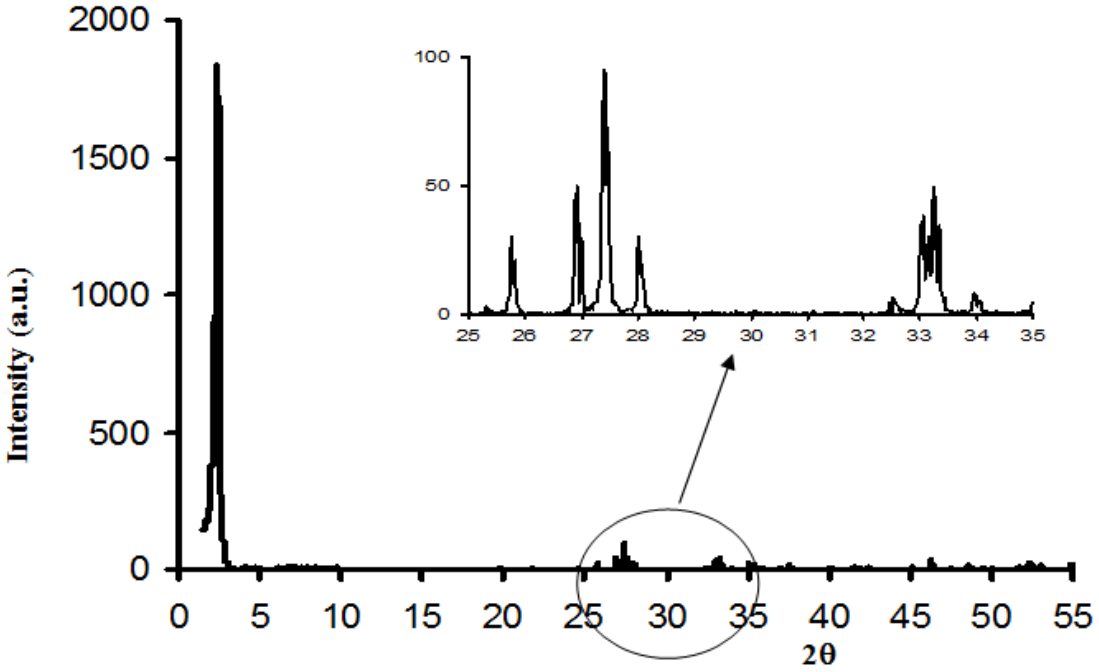


**Fig. 2.** XRD pattern of 10% $Bi_2O_3$/MCM-41 nanocomposite.

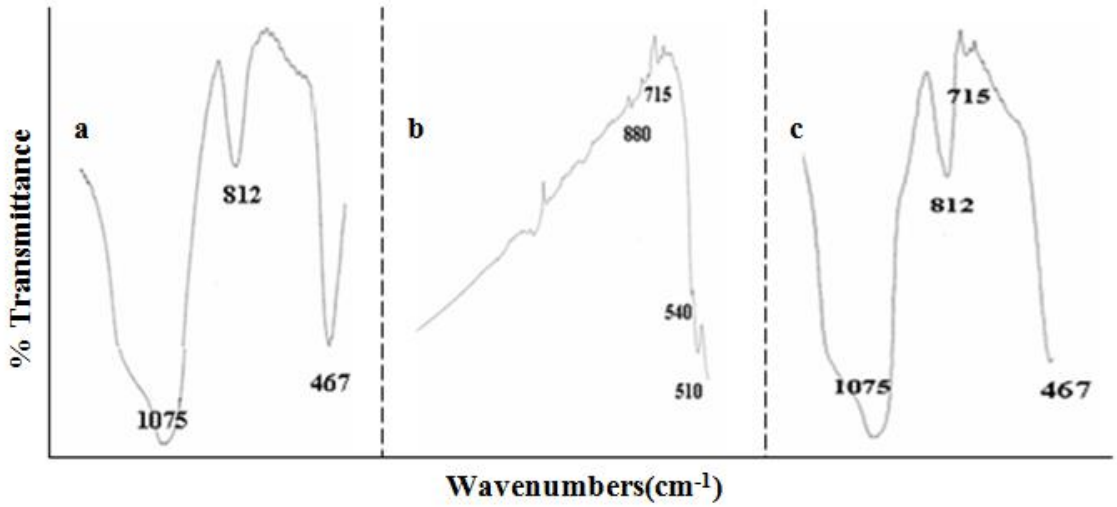


**Fig. 3.** FT-IR spectra of: (a) MCM-41 (b)$Bi_2O_3$ (c) 10% $Bi_2O_3$/MCM-41.

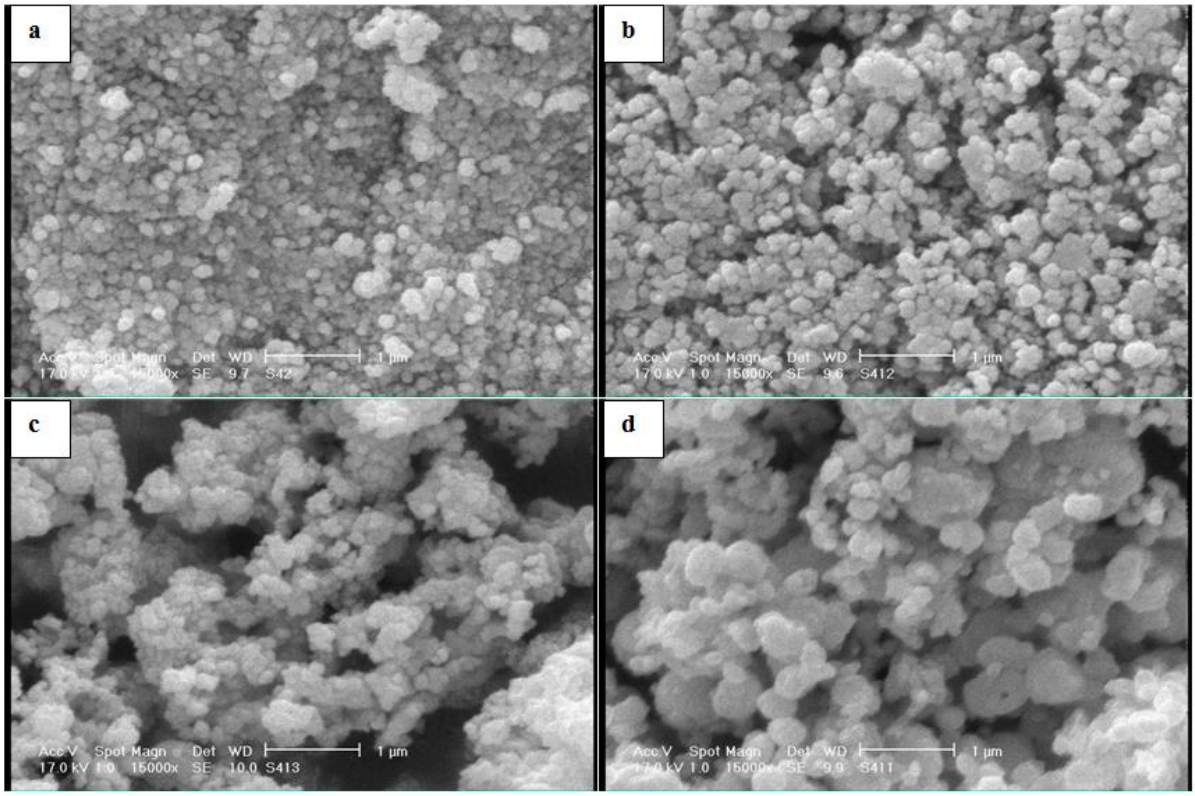


**Fig. 4.** SEM images of (a) MCM-41 (b) 5% $Bi_2O_3$/MCM-41 (c) 10% $Bi_2O_3$/MCM-41 (d) 15% $Bi_2O_3$/MCM-41.

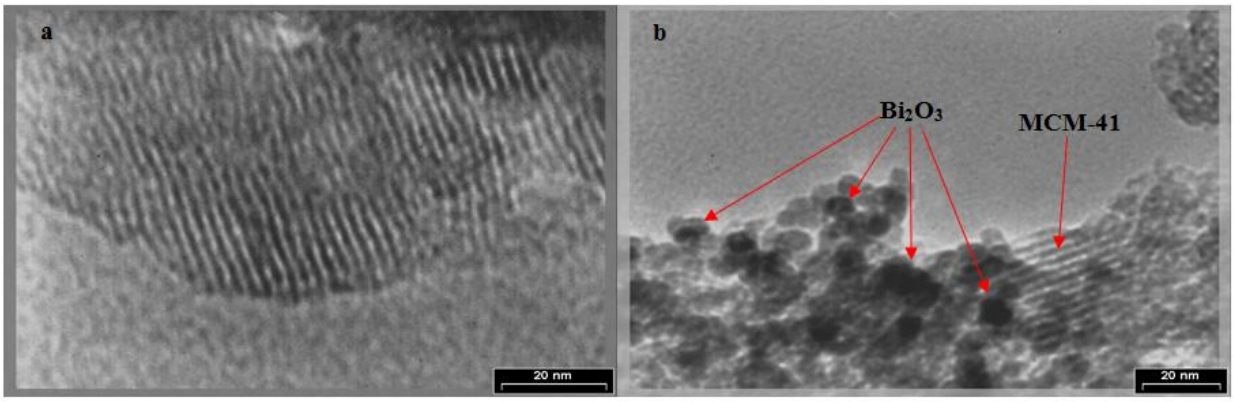


**Fig. 5.** TEM images of (a) Pure MCM-41 mesoporous and (b) 10% $Bi_2O_3$/MCM-41nanocomposite.

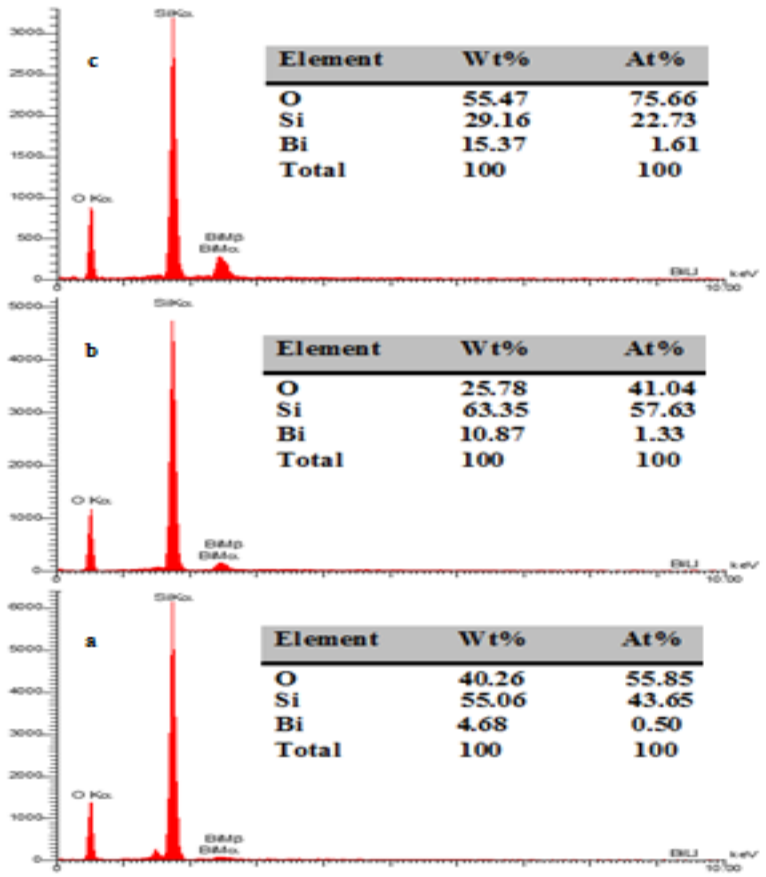


**Fig. 6.** EDAX spectrums of (a) 5% $Bi_2O_3$/MCM-41 (b) 10% $Bi_2O_3$/MCM-41 (c) 15% $Bi_2O_3$/MCM-41 nanocomposite.

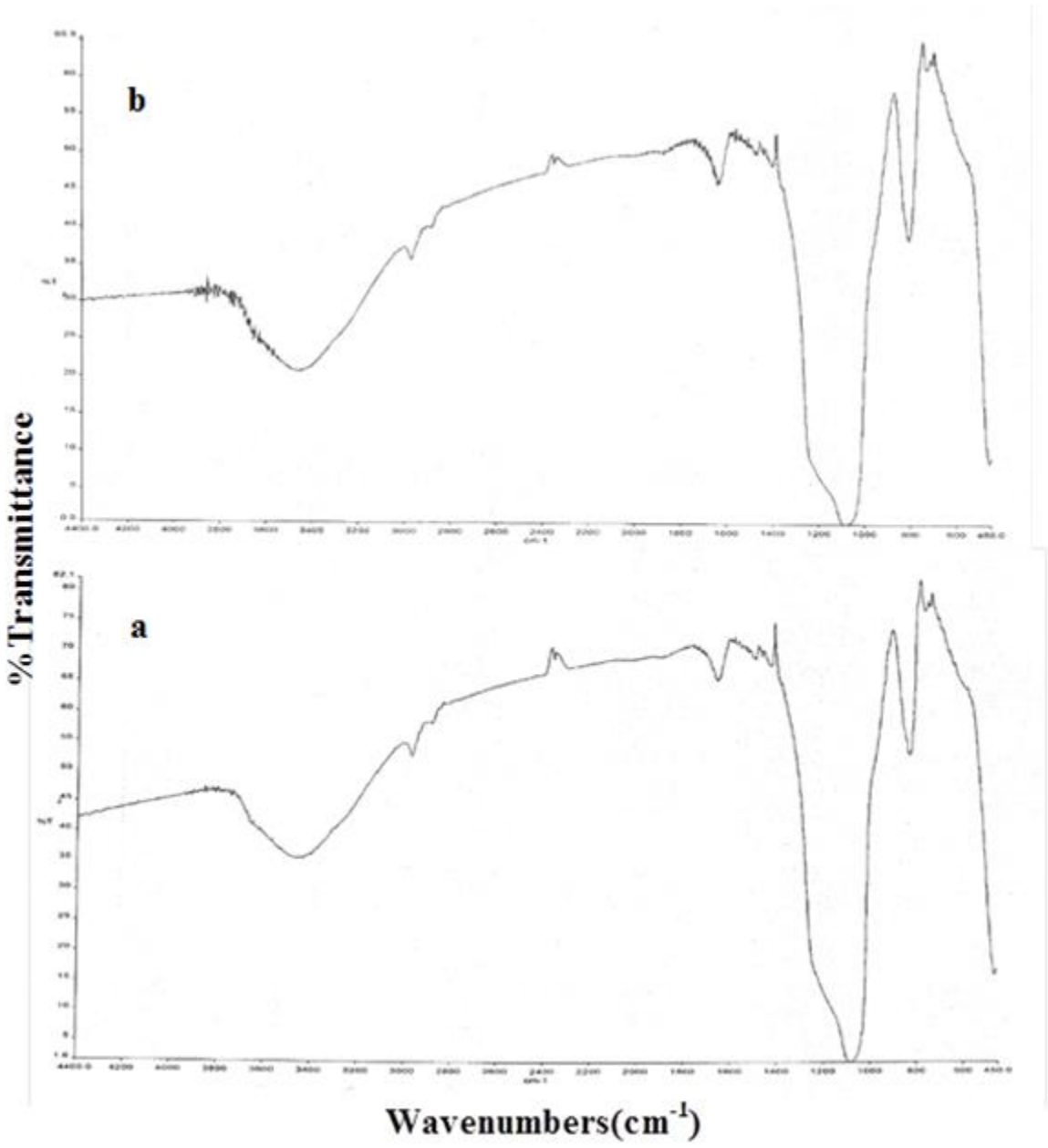


**Fig. 7.** FT-IR spectra of (a)fresh (b)used 10% $Bi_2O_3$/MCM-41 nanocomposite.

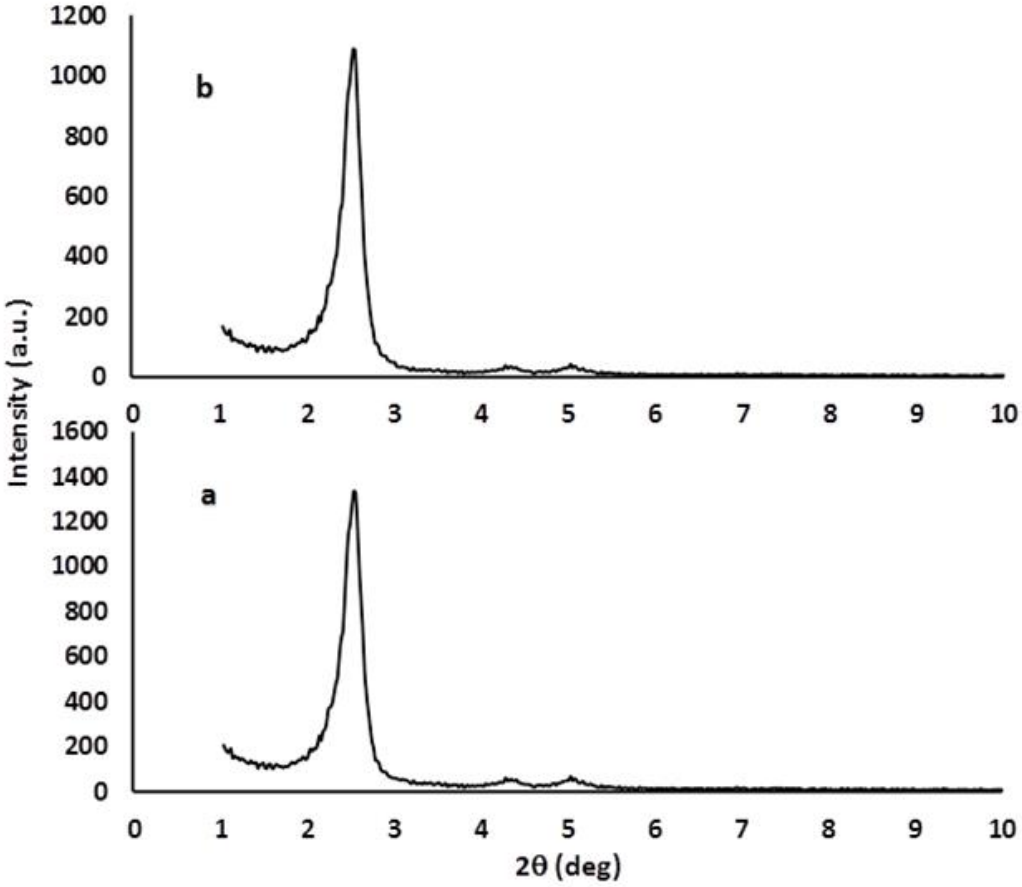


**Fig. 8.** Low-angle X-ray diffraction patterns of (a) fresh (b) used 10% $Bi_2O_3$/MCM-41 nanocomposite.

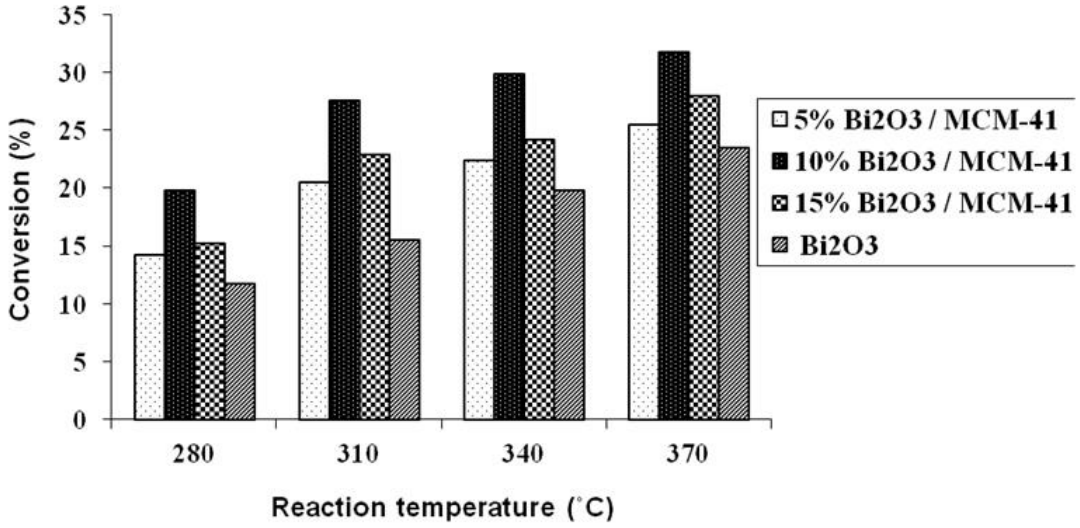


**Fig. 9.** The changes of cyclohexane conversion with respect to the reaction temperature[a].[a] Catalyst = X% $Bi_2O_3$/MCM-41 nanocomposites, catalyst weight = 1 g, reaction time = 3 h, P = 1 atm, rate of cyclohexane injection = 2 mL/h and rate of air flow = 30 mL/min

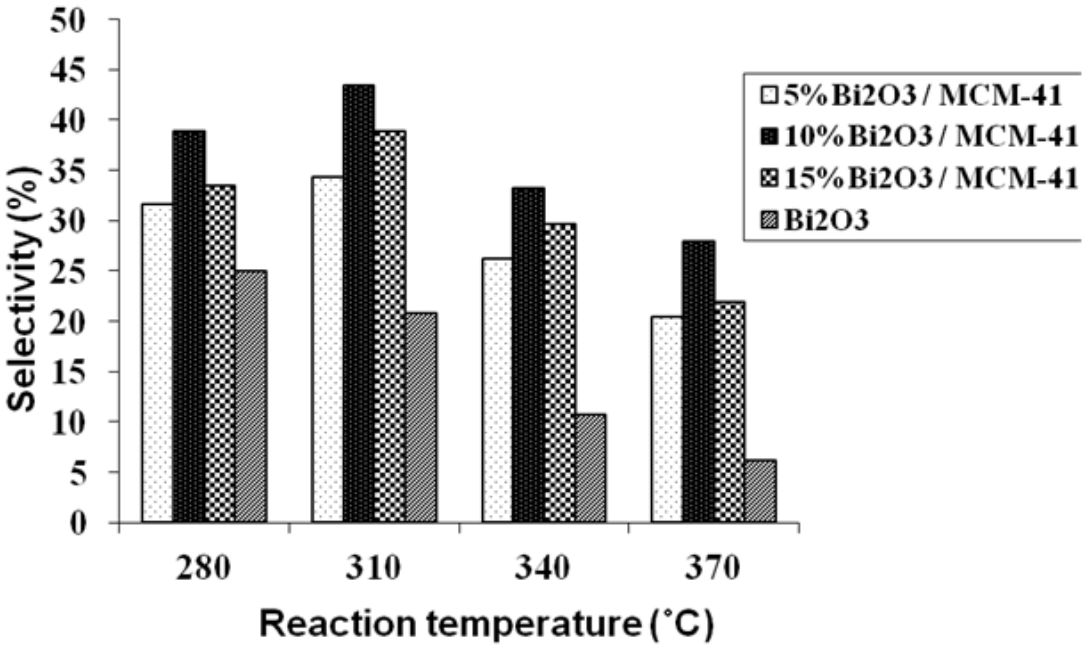


**Fig. 10.** The effect of reaction temperature on selectivity of cyclohexanone and cyclohexanol in the presence of different nanocomposites[a].[a] Catalyst = X% $Bi_2O_3$/MCM-41 nanocomposites, catalyst weight = 1 g, reaction time = 3 h, P = 1 atm, rate of cyclohexane injection = 2 mL/h and rate of air flow = 30 mL/min

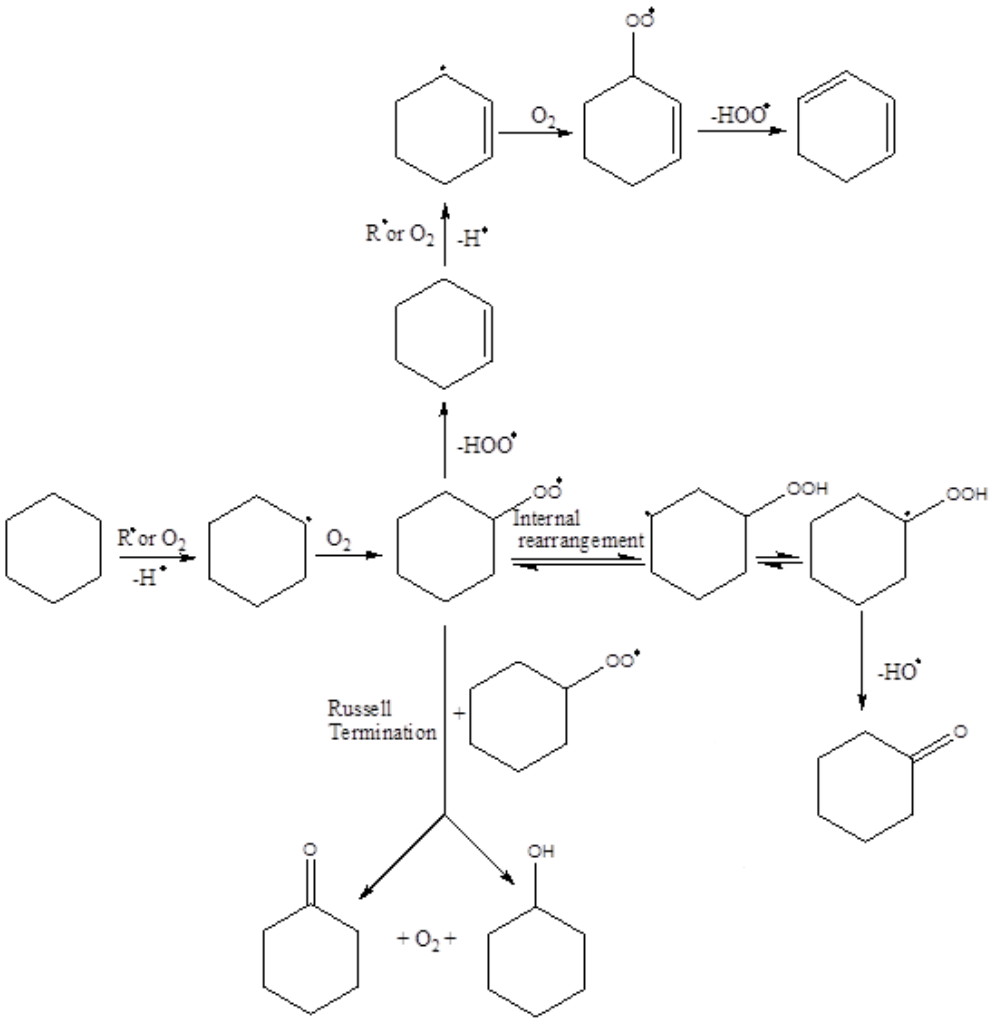


**Scheme 1.** The radical-chain sequence mechanism proposed for the oxidation of cyclohexane by $Bi_2O_3$/MCM-41 nanocomposites.